The 16th Symposium on Polar Science

2-5 December 2025

National Institute of Polar Research Research Organization of Information and Systems

Session OS

Space and Upper Atmospheric Sciences

Abstracts

Conveners: Akira Sessai Yukimatu, and Yoshimasa Tanaka (NIPR)

Global Fitting Analysis of Forbush decreases

¹ K. Munakata, ¹ Y. Hayashi, ¹ C. Kato, ² M. Kozai, ³ R. Kataoka, ^{2,4} A. Kadokura and the GMDN collaboration
¹ Faculty of Science, Shinshu University, Nagano 390-8621, Japan
² PEDSC/ROIS-DS, Tachikawa, Tokyo 190-8518, Japan
³ Science and Technology Group, OIST, Onna-son, Okinawa 904-0495, Japan
⁴ National Institute of Polar Research, Tachikawa, Tokyo 190-8518, Japan

We present the Global Fitting Analysis (GFA) of Forbush Decreases (FDs). The GFA is capable of deriving the cosmic ray density (or omnidirectional intensity), anisotropy and the spatial gradient of cosmic ray density, each as a function of time and rigidity. In this paper, we review these parameters obtained on hourly-basis for 14 FDs including three major events in May and October 2024 and in June 2025, which were also observed by the Syowa Antarctic cosmic-ray detectors.

Report on the updated cosmic ray observation at Syowa Station in 2025 and a real-time monitoring of cosmic ray rigidity spectrum using paired neutron monitor and muon detector

Y. Hayashi¹, C. Kato¹, R. Kataoka², M. Kozai³, A. Kadokura³, S. Miyake⁴, K. Murase⁵ and K. Munakata¹

¹Department of Physics, Shinshu University, Matshumoto, Nagano 390-8621, Japan

²Okinawa Institute of Science and Technology, Okinawa, Japan

³Polar Environment Data Science Center, Joint Support-Center for Data Science Research, Research Organization of Information and Systems, Tachikawa, Tokyo 190-8518, Japan

⁴National Institute of Technology (KOSEN), Gifu College, Motosu-city, 501-0495, Japan

⁵Kitami Institute of Technology, 165 Koen-cho, Kitami-shi, Hokkaido 090-8507, Japan

Syowa Station was started simultaneous cosmic ray observations with neutron monitor and muon detector in 2018. The detector system was updated by doubling the detection area of muon detector by the 66th Japanese Antarctic Research Expedition team, and started its operation in February 2025. The observed cosmic ray intensity varies responding to the space weather variation, such as the arrival of the interplanetary coronal mass ejections (ICMEs) and the corotating interaction regions (CIRs) at Earth. Forbush decrease, which is a temporal and sudden variation of cosmic ray flux, is a well-known phenomenon. While the Forbush decreases event, the cosmic ray rigidity spectrum also dynamically varies. Variations in the rigidity spectrum are important for understanding physical mechanisms responsible for the Forbush decrease. We demonstrate that the simple fraction of neutron monitor count rate is a good real-time indicator of the temporal variations of the cosmic ray rigidity spectrum, based on the analysis of major Forbush decreases occurred recently. In this talk, we also report on current status and possible future upgrade of the observation.

Cosmic-ray Muon Observation Plan in Iceland

Masayoshi Kozai¹, Akira Kadokura¹, Chihiro Kato², Kazuoki Munakata², Naoko Miyashita², Yuki Hayashi², Ryuho Kataoka³, Shoko Miyake⁴, Kiyoka Murase⁵ and Yoshimasa Tanaka^{1,6}

¹Polar Environment Data Science Center, Joint Support-Center for Data Science Research, Research Organization of Information and Systems, Tokyo, Japan

²Faculty of Science, Shinshu University, Nagano, Japan

³Science and Technology Group, Okinawa Institute of Science and Technology, Okinawa, Japan

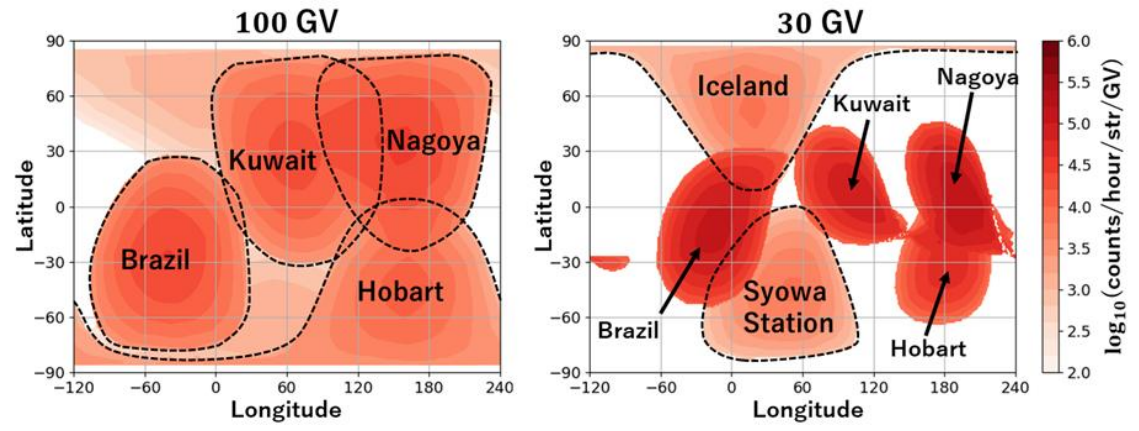
⁴National Institute of Technology (KOSEN), Gifu College, Gifu, Japan

⁵Faculty of Engineering, Kitami Institute of Technology, Hokkaido, Japan

⁶National Institute of Polar Research, Research Organization of Information and Systems, Tokyo, Japan

The momentum-space distribution function of galactic cosmic-rays (GCRs) is observed as their anisotropy at Earth, enabling us to probe three-dimensional solar wind structures based on the GCR transport theory. Thanks to the high penetration power of cosmic-ray muons in the atmosphere, ground-based muon detectors feature an excellent angular resolution, angular acceptance, and statistics for GCRs, all essential to measure the anisotropy. The Global Muon Detector Network (GMDN) [1] has been a unique experiment deploying muon detectors worldwide to secure high sensitivity to the anisotropy. GMDN started with two-hemisphere observations in Nagoya (Japan) and Hobart (Australia) in the 90s, and the core 4-station network was established in the 2000s by initiating São Martinho da Serra (Brazil) and Kuwait stations. The initial goal of construction was achieved in 2016 by expanding the Kuwait detector.

The completed GMDN is shedding new light on GCR anisotropy, but there are still limitations in the observation network. The geomagnetic field deflects GCR trajectories, causing the muon detector's viewing direction to be biased eastward and toward the opposite hemisphere in Earth's magnetosphere. This effect prevents low- and midlatitude detectors from observing high-latitude directions, especially for low-rigidity GCRs. Only muon detectors in the geographic polar region are sensitive to low-rigidity GCRs incoming from high-latitude directions. The figure shows the viewing directions of each GMDN detector and a virtual detector in Iceland, derived from GCR transport simulations in the magnetosphere and atmosphere. It is demonstrated that a nearly all-sky field of view is achieved only by mid-latitude detectors for 100 GV GCRs (left panel), but they are shrunk into low-latitude directions for 30 GV GCRs (right panel). The polar detectors cover these high-latitude and low-rigidity observation gaps well.



We are planning to install a muon detector in Iceland, and its polar conjugate observation with the Syowa Station detector, which was started in 2018, will address this insensitive region. In addition, constraints specific to the Icelandic observation site, unlike those at other GMDN stations, enable us to demonstrate a new design concept, such as a field-deployable or portable observation unit. We also demonstrated the conversion of muon observation data into the Common Data Format, and its publication through IUGONET [2] with a data analysis tool [3], aiming to establish an end-to-end data pipeline. We will report on these activities related to the Iceland observation plan.

References

- [1] http://hdl.handle.net/10091/0002001448
- [2] https://search.iugonet.org/metadata/001/00003723
- [3] https://doi.org/10.5281/zenodo.15844859

CO₂-Driven Shifts in Sporadic E Formation from GAIA Simulations

Farhan Naufal Rifqi¹, Huixin Liu¹, Lihui Qiu², Chihiro Tao³, and Hiroyuki Shinagawa²

¹Department of Earth and Planetary Sciences, Kyushu University, Fukuoka, Japan

²International Research Center for Space and Planetary Environmental Science (i-SPES), Kyushu University, Fukuoka, Japan

³National Institute of Communication and Technology, Tokyo, Japan

Using the Ground-to-topside model of Atmosphere and Ionosphere for Aeronomy (GAIA), the study assesses how increasing CO₂ level alters sporadic E (Es) formation via analysis of vertical ion convergence (VIC). Under a doubled-CO₂ experiment, simulations indicate a pronounced enhancement in VIC between 100–120 km. This suggests the lowering of Es formation altitudes, pointing to a future shift of Es occurrence patterns in a warming climate. The amplification of VIC is primarily linked to CO₂-driven reduction in the ion-neutral collision frequency, alongside changes in zonal wind shear. Taken together, the results suggest that anthropogenic climate change enhances ion convergence processes and is likely to raise the frequency of Es events.

Impact of increasing CO2 on upper atmosphere response to a May 2024 - like Superstorm

Huixin Liu¹, Nick Pedatella²

¹Kyushu University, Japan

²National center for atmospheric research, US

The Community Earth System Model (CESM) Whole Atmosphere Community Climate Model with thermosphere-ionosphere eXtension (WACCM-X) is used to investigate how the ionosphere-thermosphere response to a May 2024-like geomagnetic storm changes with increasing greenhouse gases. Coupled CESM(WACCM-X) simulations are first performed following the Coupled Model Intercomparison Project Phase 6 Shared Socioeconomic Pathway 5–8.5 from 2000 to 2090. The May 2024 geomagnetic superstorm is then simulated in 2016, 2040, 2061, and 2084, corresponding to surface CO2 levels of 403, 500, 652, and 918 ppmv, respectively. The CESM(WACCM-X) simulations indicate that increasing levels of CO2 weakens the absolute neutral density response at 350 km. However, the relative response is increased with increasing levels of , which is partly due to the decrease in the background neutral density. Due to a weaker response in thermosphere composition and meridional neutral winds, the ionospheric response in absolute terms also weakens with increasing levels of CO2.

Correction of Temperature Data from Super-pressure Balloon Observations in the Antarctic Region

Rina Kawakami¹ and Yoshihiro Tomikawa^{2,1}

¹ The Graduate University for Advanced Studies, SOKENDAI

² National Institute of Polar Research

Atmospheric gravity waves (GWs) are atmospheric waves driven by buoyancy forces. They transport momentum and energy over long distances and contribute to driving the global-scale meridional circulation. GWs play a crucial role in determining wind, temperature, and material distributions, particularly in the middle atmosphere at altitudes of 10–100 km. Understanding the spatiotemporal structure of momentum transport by GWs is therefore essential. However, their spatial scales range from several kilometers to thousands of kilometers, and their timescales span from minutes to tens of hours. Capturing the complete sequence of GW excitation, propagation, and dissipation, and quantitatively evaluating their role in driving the meridional circulation, remains challenging even with the latest observations and models. The Antarctic region is especially active for GWs but also difficult to observe, representing the location of greatest uncertainty in models.

To address this issue, the LODEWAVE project was conceived to conduct GW observations in Antarctica using super-pressure (SP) balloons [Tomikawa et al., 2023]. SP balloons maintain internal pressure higher than ambient atmospheric pressure, preventing buoyancy fluctuations between day and night and enabling extended flight durations (>1 month).

LODEWAVE has conducted two observation campaigns to date. The first campaign took place at Syowa Station, Antarctica, from January to February 2022. Although it achieved a maximum flight duration of three days, accurate temperature data could not be obtained. In SP balloon observations, where ventilation during flight is nearly zero, thermistors tend to be heated by solar radiation, leading to a significant overestimation of atmospheric temperature [Hertzog et al., 2004]. A similar effect was observed in LODEWAVE. In addition, thermistors received heat flux from the balloon envelope, introducing short-period fluctuations. To address these issues, improvements were implemented for the second campaign; however, it was not possible to completely eliminate the effects of solar radiation and heat flux.

Accurate temperature data are essential for GW analysis and model data assimilation. In this study, we applied corrections for the effects of solar radiation and heat flux from the housing to improve the accuracy of temperature data obtained from SP balloon observations. After correction, the observed data showed reduced deviations from atmospheric reanalysis data, successfully mitigating the influence of heat flux and solar radiation. Furthermore, high-frequency components not captured in the reanalysis data were detected, suggesting the presence of atmospheric GW signals.

References

Hertzog A, et al., 2004, Quarterly Journal of the Royal Meteorological Society, 130, 607-626. Tomikawa, Y., et al. (2023), LODEWAVE (Long-Duration balloon Experiment of gravity WAVE over Antarctica), J. Evolv. Space Activ., 1, 14.

Comparative Analysis of All-Sky Camera Images and Infrasound Signals to Identify Aurora-Associated Events

<u>Hinata Asano¹</u>, Masa-yuki Yamamoto¹ ¹Kochi University of Technology

Observing infrasound generated by natural phenomena in the upper atmosphere is crucial for understanding its three-dimensional propagation characteristics. The potential association between auroral activity and infrasound has been suggested since the work of Wilson (1969), who conducted observations using infrasound and magnetic field measurements, although no conclusive correlation was established. More recently, Ohata (2020) attempted to identify aurora-related infrasound at Showa Station, Antarctica, by comparing the infrasound dataset (Kanao, 2008) with All-sky Color Digital Camera images (Miyaoka et al., 2005). However, the study period coincided with a solar minimum, resulting in limited events and inconclusive findings.

In this study, we applied the comparative analysis framework developed by Ohata (2020) to data collected at Syowa Station during March–May 2024, a period of high solar activity and frequent auroral occurrences. The dataset included infrasound observations with Nanobarometer (6000-16B), all-sky camera images (captured at 1-second intervals), and meteorological wind speed data derived from the database. We computed the degree of temporal variation in the auroral emission as the number of pixels differing by more than 20% between consecutive frames, and compared this metric with band-pass filtered (0.01–0.1 Hz) infrasound waveforms. As a result, the characteristic waveform, considered to be associated with the auroral activities, was observed approximately 3-5 minutes after a change in the degree of temporal variation in six independent events.

Future work will involve FK analysis to determine the arrival directions of the infrasound signals and cross-correlation analysis to evaluate their quantitative similarity with the degree of temporal variation in the aurora borealis. These preliminary results provide new observational evidence for aurora-associated infrasound, serving as a basis for further discussion on the coupling mechanisms between rapidly moving auroral processes and the atmosphere.

References

Charles R. Wilson (1969), Auroral Infrasonic Waves, *Journal of Geophysical Research, Space Physics*, **74**, pp. 1812-1836.

Haruka Ohata (2020), Establishment of investigating methods for clarifying the correspondence between infrasound in the polar regions and natural phenomena such as the aurora, *Polar Science Symposium*, OMp29, Tachikawa.

Masaki Kanao (2008), Infrasound digital records at Syowa Station, *National Institute of Polar Research*. Hiroshi Miyaoka (2005), Akira Kadokura (since 2020), Color Digital Camera (CDC) at Syowa Station, *National Institute of Polar Research*.

Poleward Disturbances in Thermospheric Winds during the 3-4 November 2021 Geomagnetic Storm

<u>Jonna Wehmeyer ^{1,2}</u>, Yoshihiro Tomikawa^{2,1,3}, Takanori Nishiyama^{2,1}, Yasunobu Ogawa^{2,1,3} and Eframir Franco-Diaz⁴

¹The Graduate University for Advanced Studies, SOKENDAI, Hayama, Kanagawa, Japan

²Institute of Polar Research, Tachikawa, Tokyo, Japan

³Polar Environment Data Science Center, Joint Support-Center for Data Science Research, Tachikawa, Tokyo, Japan

⁴Computational Physics Inc., Lafayette, CO, U.S.A.

During geomagnetic storms, particle and Joule heating in the auroral zone cause an expansion of the polar atmosphere which induces strong equatorward thermospheric winds at high and middle latitudes. These winds are important drivers of the ionospheric disturbance dynamo which greatly influences the response of the low latitude ionosphere to geomagnetic storms. However, previous studies reported that these equatorward winds are occasionally interrupted by surges of poleward wind, and it has been suggested that these poleward surges might affect the evolution of the ionospheric disturbance dynamo. Although poleward surges have been repeatedly reported, there is controversy about what causes them and even the basic characteristics of poleward surges are still widely unestablished. Therefore, further research is needed to classify characteristics and generation mechanisms of poleward surges.

This study focuses on a poleward surge observed at mid-latitudes over North America during the 3-4 November 2021 strong geomagnetic storm (Kp 8-). We comprehensively analyze storm-time ionospheric and thermospheric disturbances using data from ground-based instruments at Poker Flat (65.12 degrees geographic latitude), Millstone Hill (42.37 degrees geographic latitude), and Urbana (40.13 degrees geographic latitude), as well as satellite observations and model data. The poleward surge was observed at Millstone Hill (50 m/s) and Urbana (75 m/s) on November 4, when both stations were located in the magnetic local time (MLT) post-midnight sector. The poleward surge at Millstone Hill was preceded by an equatorward surge (-300 m/s). Previous studies suggested Traveling Atmospheric Disturbances (TADs) as most likely cause for poleward surges but for this event neither equatorward nor poleward surges concurred with Large-scale Traveling Ionospheric Disturbances (LSTIDs), that would indicate the presence of TADs. Instead, a Subauroral Polarization Stream (SAPS) with ion velocities greater than -1500 m/s accompanied by a deep ionospheric trough moved to latitudes as low as 40 degrees geographic latitude and was located close to Millstone Hill and Urbana when the equatorward and poleward surges were observed. The region around the SAPS is heavily influenced by ion drag of the SAPS and pressure gradients due to collisional heating that accelerate neutral winds in different directions depending on their position relative to the SAPS. Therefore, we propose that the extreme disturbances in meridional winds were mainly caused by SAPS forcing, rather than equatorward propagating TADs. The MLT location of Millstone Hill and Urbana indicates that during the disturbances both stations were located within the eastward backflow sector of the SAPS, which likely contributed to the complicated ion-neutral dynamics.

References

Aa, E., Zhang, S., Erickson, P., Coster, A., Goncharenko, L., Varney, R., & Eastes, R. (2021). Salient midlatitude ionosphere-thermosphere disturbances associated with saps during a minor but geo-effective storm at deep solar minimum. Journal of Geophysical Research: Space Physics. doi: 10.1029/2021ja029509

Blanc, M., & Richmond, A. (1980). The ionospheric disturbance dynamo. doi: 10.1029/ja085ia04p01669

Guo, J., Deng, Y., Zhang, D., Lu, Y., Sheng, C., & Zhang, S. (2018). The effect of subauroral polarization streams

Guo, J., Deng, Y., Zhang, D., Lu, Y., Sheng, C., & Zhang, S. (2018). The effect of subauroral polarization streams on ionosphere and thermosphere during the 2015 st. patrick's day storm: Global ionosphere-thermosphere model simulations. doi: 10.1002/2017ja024781

Shiokawa, K., Otsuka, Y., Ogawa, T., Kawamura, S., Yamamoto, M., Fukao, S., . . . Yumoto, K. (2003). Thermospheric wind during a storm-time large-scale traveling ionospheric disturbance. doi: 10.1029/2003ja010001

Zhang, K., Wang, H., Wang, W., Liu, J., Zhang, S., & Sheng, C. (2021). Nighttime meridional neutral wind responses to saps simulated by the tiegcm: A universal time effect. Earth and planetary physics. doi: 10.26464/epp2021004

Zhang, S., Erickson, P., Foster, J., Holt, J., Coster, A., Makela, J., . . . Kerr, R. (2015). Thermospheric poleward wind surge at midlatitudes during great storm intervals. doi: 10.1002/2015gl064836

Interhemispheric comparison of long-term variation of geomagnetic activity at Syowa-Iceland conjugate stations

Akira Kadokura^{1,2}, and Gunnlaugur Bjornsson³
¹Polar Environment Data Science Center, ROIS-DS

²National Institute of Polar Research

³University of Iceland

Long-term variation of geomagnetic activity at Syowa Station (SYO) (S69.00 deg) in Antarctica and Leirvogur (LRV) (N64.18 deg) in Iceland was investigated. Both SYO and LRV are located at auroral latitudes and in a unique geomagnetic conjugate relationship with each other. Geomagnetic variation data from 1966 until 2024 at LRV and SYO, respectively, were used for this analysis. Using those over five solar cycle data, similarity and dissimilarity in the solar cycle variation, seasonal variation, and diurnal variation of geomagnetic activity at those conjugate stations were investigated to understand interhemispheric difference in auroral activity responding to the variation of the solar wind input and solar activity. Following results were obtained so far:

- 1. Activity at LRV gradually decreased, relatively to one at SYO. Before and after around 1984-1989, magnitude at LRV was larger and smaller than SYO, respectively, which could be due to the long-term variation of the geomagnetic latitude at LRV toward the lower latitudes.
- 2. A significant difference between SYO and LRV was observed in 1980 and 1982, when the activity was much more quiet at SYO than LRV.
- 3. Activity peak around equinox period can be seen more clearly in the nightside hours, while winter-summer difference is more clear in the dayside.
- 4. Maximum activity in the nightside during equinox period can be seen in spring, during 21-24 UT in March and 00-03 UT in April, which could be related with the lowest ionospheric conductivity in both hemispheres.
- 5. Peak of the summer-winter difference in the dayside shifts post-noon hours due to the difference in local times at both stations.
- 6. In the nightside, a reversed sense winter-summer variation can be seen in the activity difference between LRV and SYO, which could be related with the conductivity difference between winter hemisphere and summer hemisphere, i.e., geomagnetic activity in the nightside is more active in winter hemisphere than in summer hemisphere.

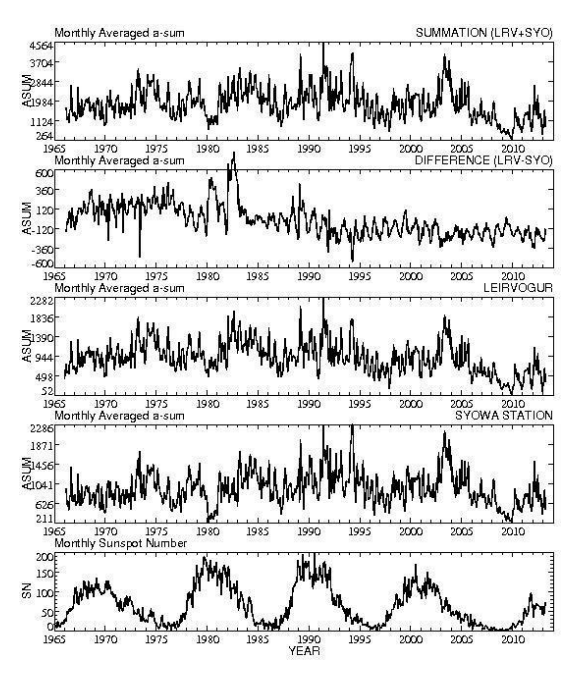


Fig. 1. Long-term variation of sunspot number, and monthly-averaged a-index at SYO and LRV.

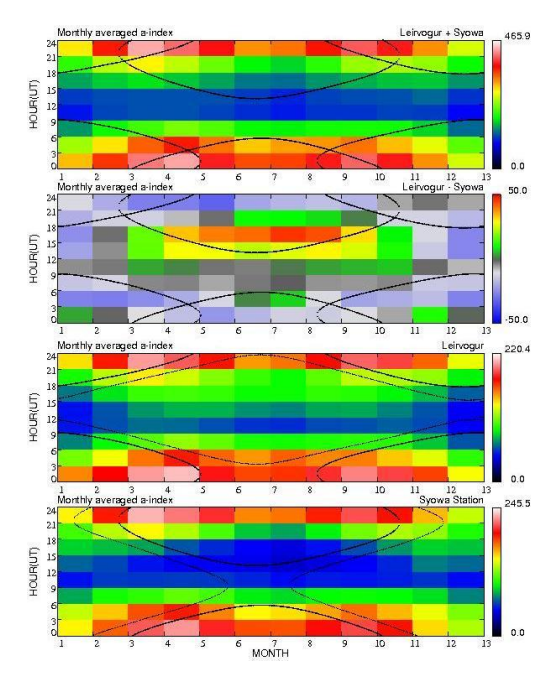


Fig. 2. Annual and daily variation of monthly averaged a-index during whole period.

South-North Conjugate Observations of Pulsating Auroras with Arase Satellite

Yuri Ito^{1,2}, Yasunobu Ogawa^{2,1}, Yoshimasa Tanaka^{2,1,3}, Akira Kadokura^{2,3}, Mizuki Fukizawa^{2,1},
Mitsunori Ozaki⁴, Keisuke Hosokawa⁵, Yoshizumi Miyoshi⁶, Yoshiya Kasahara⁴, Shoya Matsuda⁴,
Satoshi Kasahara⁷, Shoichiro Yokota⁸, Kunihiro Keika⁷, Tomoaki Hori⁶, Ayako Matsuoka⁹,

Mariko Teramoto¹⁰, Kazuhiro Yamamoto⁶, and Iku Shinohara¹¹

¹The Graduate University for Advanced Studies, SOKENDAI

²National Institute of Polar Research

³Research Organization of Information and Systems, Joint Support-Center for Data Science Research

⁴Kanazawa University

⁵University of Electro-Communications

⁶Institute for Space-Earth Environmental Research, Nagoya University

⁷University of Tokyo

⁸Osaka University

⁹Kyoto University

¹⁰Kyushu Institute of Technology

¹¹Institute of Space and Astronautical Science, JAXA

Tjornes in Iceland and Syowa station in Antarctica are the few north-south conjugate points connected by the same magnetic field lines. We conduct all-sky images, VLF, ULF, and riometer observations in Tjornes and all-sky images, VLF, ULF, riometer, millimeter-wave, and PANSY observations at Syowa station, which mean comprehensive ground-based observational capabilities. Previous studies have leveraged the advantage to investigate the north-south conjugacy of auroras, as well as pulsating auroras (PsA). Among auroras, south-north asymmetric traveling surges and conjugacy/non-conjugacy of PsAs have been reported [Uchida et al., 2020; Sato et al., 1998; Fujii et al., 1987]. In our previous study, we have observationally proposed a physical process in which wave propagation latitudes, the energy of scattered electrons, and patchy structure of PsA are controlled by "density ducts". We consider density ducts to exist in the magnetosphere as tube-flux connecting the southern and northern hemispheres. Thus, we can speculate south-north conjugacy of PsA patches caused by magnetospheric density ducts. However, there has been no previous study of south-north conjugate observations focusing on the relationship between PsA conjugacy and density ducts.

A south-north conjugate event on September 22, 2018, from 22:30 to 23:10 UT is valuable because similar PsAs were simultaneously observed in both hemisphere sides, with magnetospheric observations conducted by the Arase satellite at high latitude region of -23°. During PsAs, Arase observed chorus wave propagating towards higher latitudes and ~90 keV electrons precipitating into the ionosphere of both hemispheres. The observations have provided the first direct evidence of chorus waves originating near the magnetic equator that propagate and scatter electrons in both hemispheres while simultaneously occurring PsAs in both southern and northern hemispheres. In this presentation, we report the preliminary results of this event with data of images, waves, and particles, and discuss the relationship between PsAs and density ducts.

References

Uchida, H. A., R. Kataoka, A. Kadokura, K. Murase, A. S. Yukimatu, & Y. Miyoshi, et al., Asymmetric development of auroral surges in the Northern and Southern Hemispheres. Geophysical Research Letters, 47, e2020GL088750, https://doi.org/10.1029/2020GL088750, 2020.

Sato, N., M. Morooka, H. Minatoya, and Th. Saemundsson, Nonconjugacy of pulsating auroral patches near L=6, Geophysical Research Letters, 25, 3755-3758, https://doi.org/10.1029/1998GL900002, 1998.

Fujii, R., N. Sato, T. Ono, H. Fukunishi, T. Hirasawa, S. Kokubun, T. Araki, and Th. Saemundsson, Conjugacies of pulsating auroras by all-sky TV observations, Geophysical Research Letters, 14, 115-118, https://doi.org/10.1029/GL014i002p00115, 1987.

Ito, Y., Hosokawa, K., Ogawa, Y., Miyoshi, Y., Tsuchiya, F., Fukizawa, M., et al. On the factors controlling the relationship between type of pulsating aurora and energy of pulsating auroral electrons: Simultaneous observations by Arase satellite, ground-based all-sky imagers and EISCAT radar. Journal of Geophysical Research: Space Physics, 129, e2024JA032617. https://doi.org/10.1029/2024JA032617, 2024.

Estimation of the Precipitating Electron Energy Spectrum from Three-Dimensional Electron Density Observations

Mizuki Fukizawa^{1, 2}, Yasunobu Ogawa^{1, 2, 3} and Yoshimasa Tanaka^{1, 2, 3}

¹ National Institute of Polar Research

² The Graduate University for Advanced Studies, SOKENDAI

³ Polar Environment Data Science Center, ROIS-DS

The CARD method, which estimates the energy spectrum of precipitating electron flux from the E-region electron density altitude distribution observed by the European Incoherent Scatter (EISCAT) radar, has been developed and widely applied (Brekke et al., 1989; Fujii et al., 1995). However, the current EISCAT system employs a large-aperture antenna and effectively performs single-direction observations, restricting spectral estimation to a single magnetic-zenith point. In contrast, the forthcoming EISCAT_3D radar will utilize a phased-array antenna to enable simultaneous three-dimensional observations of the ionosphere. This study therefore aims to develop a method for estimating the two-dimensional horizontal distribution of the precipitating electron-flux energy spectrum from the three-dimensional electron-density data provided by EISCAT_3D.

We assumed a discrete auroral arc as the true-value model and constructed an energy distribution by adding one-sided power-law components to the low- and high-energy sides of a Gaussian characteristic-energy profile. The spatial distribution of total energy flux was represented by a Gaussian function in the north-south direction with a uniform offset. In the east-west direction, the center of this north-south Gaussian was allowed to meander sinusoidally. This energy spectrum was placed both at the magnetic zenith of the transmitter station and 50 km to its low-latitude side, with characteristic energies set to 3 keV on the high-latitude side and 5 keV on the low-latitude side. The energy range was defined as 1–50 keV. From this prescribed true-value spectrum, a three-dimensional electron density distribution was generated by solving the electron-density continuity equation under steady-state conditions, incorporating models for the ionization rate, neutral atmosphere, and effective recombination coefficient. We then sampled the resulting electron density using the 27-beam configuration planned for the EISCAT_3D Common Programme, added observational noise, and produced simulated observational data. Because estimation of the precipitating electron spectrum requires the electron-density altitude profile along magnetic field lines, we employed the coordinate system (x, y, z) = (east, north, magnetic zenith) and performed two-dimensional interpolation of the electron-density data at the 27 beam points for each altitude plane.

While the conventional CARD method employs a least-squares approach, our technique reconstructs the spectrum using maximum a posteriori (MAP) estimation. A smoothness constraint is applied by minimizing the second derivative of the electron flux with respect to energy. The results confirmed that the energy spectrum of precipitating electrons was accurately estimated within the error bars for the arc located at magnetic zenith (A and B in Fig. 1). However, the low-energy side of the spectrum was underestimated for the low-latitude arc (C in Fig. 1). For the two-dimensional distributions of total energy flux and mean energy, the high-latitude arc was retrieved with relatively high accuracy. Conversely, the low-latitude arc exhibited an underestimation of total energy flux by up to about 8 mW m⁻² and an overestimation of mean energy by as much as 4 keV (left panels of Fig. 1). This discrepancy is likely attributable to the smaller beam-elevation angle at low latitudes relative to the magnetic zenith and to the increased observational noise at higher altitudes.

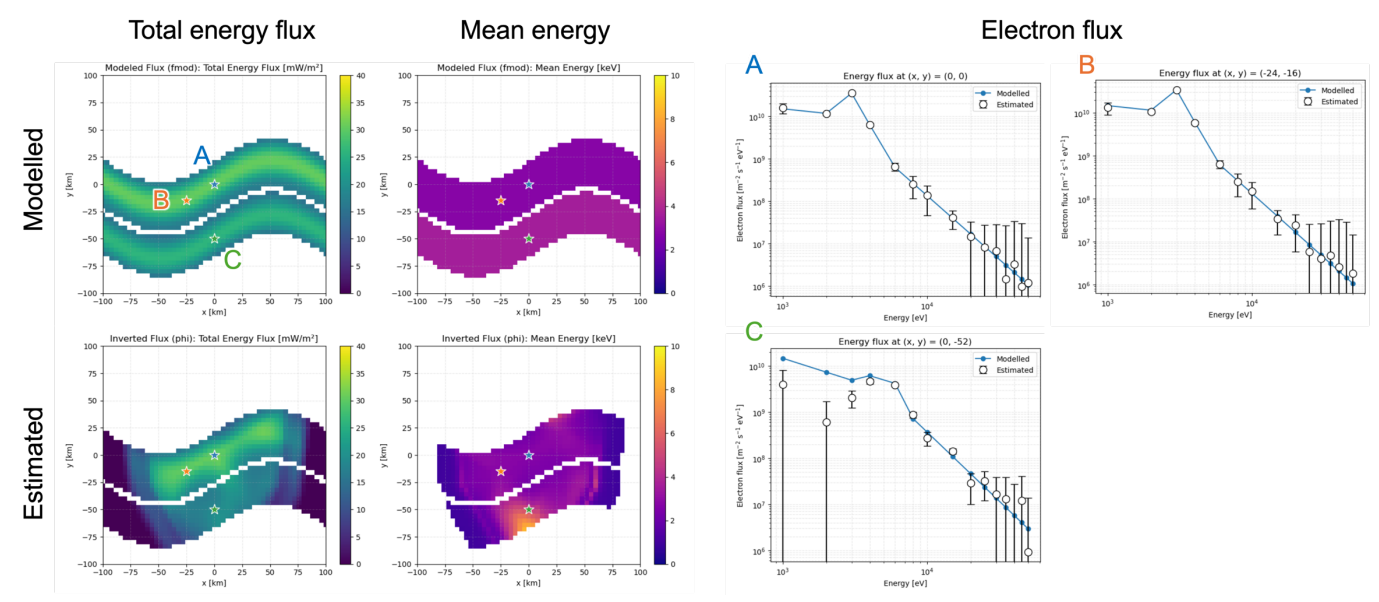


Figure 1. Estimation results of the total energy flux, mean energy, and electron flux.

References

Brekke, A., Hall, C., and Hansen, L.: Auroral ionospheric conductance during disturbed condition, Ann. Geophys., 7, 269–280, 1989.

Fujii, R., Nozawa, S., Sato, M., Matuura, N., Ono, T., Brekke, A., Hall, C., and Hansen, T. L.: Comparison between Electron Spectra Calculated from EISCAT Electron Density Profiles and Those Observed by the DMSP Satellites., Journal of geomagnetism and geoelectricity, 47, 771–782, https://doi.org/10.5636/jgg.47.771, 1995.

Stormtime electric fields at middle and low latitudes as observed by HF Doppler sounders and magnetometers during the super storm on May 10-11, 2024

<u>Takashi Kikuchi</u>¹, Kumiko K. Hashimoto², Keisuke Hosokawa², Ichiro Tomizawa², Jaroslav Chum³, Yusuke Ebihara⁴, Yukitoshi Nishimura⁵

Institute for Space-Earth Environmental Research, Nagoya University
 Department of Communication Engineering and Informatics, University of Electro-Communication
 Department of the Ionosphere and Aeronomy, Institute of Atmospheric Physics of the Czech Academy of Sciences
 Research Institute for Sustainable Humanosphere, Kyoto University
 Center for Space Physics, Boston University

The Mother's day storm on May 10-11, 2024 provided us with opportunities to confirm previously established characteristics of geomagnetic storms and to find new properties of ionospheric electric field and currents from mid-latitudes to the equator. Mid-latitude geomagnetic sudden commencement (SC) (SCx,y in X or Y component) is bipolar as SC (PI, MI), where PI and MI refer to as the preliminary impulse and main impulse, respectively. Magnetometer networks at middle latitudes observed that SCx(+ -) and SCy(- +) in the morning, and SCx(- +) and SCy(+ -) in the afternoon. The equatorial SC was SCx(-+) on the day and SCx(+-) in the night. The local time and latitude dependence of SC is consistent with that shown by Kikuchi et al. (2022a). Storm main phase magnetic field disturbances (MPx,y) at mid-latitudes are MPx(-) and MPy(+) in the morning and MPx(+) and MPy(-) in the afternoon, and MPx(+) at the equator during the day and MP(-) in the night, in the same way as the MI of SC. The local time and latitude dependence of the storm main phase magnetic disturbances is consistent with that of DP2 magnetic fluctuations (Kikuchi et al., 2022b). The PI and MI/MP are due to DP2 currents driven by the dusk-to-dawn PI and dawn-to-dusk MI/MP electric fields, respectively. DP2 currents are composed of two-cell Hall current vortices at high-middle latitudes surrounding the foot of field-aligned currents and of Pedersen-Cowling currents between the foot of field-aligned currents and equatorial ionosphere. HF Doppler sounders in Japan observed eastward PI and westward MI/MP electric fields during the night, consistent with storm main phase electric field observed by the HF Doppler sounders in Japan and Czechia (Hashimoto et al., 2020). A few hours later in the storm main phase, the electric field and currents reversed their directions, because of the overshielding due to convection reduction (Kikuchi et al., 2000). It was found that the overshielding electric field was so strong that the nighttime ionospheric F-layer over Japan rose to an altitude of 800 km. During the recovery phase of the storm on May 11 2024, several substorm positive bays occurred at mid-latitudes in the night, which are found to be associated with DP2 currents on the dayside, same as the MI/MP currents. The HF Doppler sounders detected the dawn-to-dusk convection electric fields during the stormtime substorms, in contrast to the dusk-to-dawn overshielding electric fields having often been observed during isolated substorms (Hashimoto et al., 2017). The stormtime-substorm electric field and currents remain an issue to be solved.

Reference

- Hashimoto, K. K., T. Kikuchi, I. Tomizawa, and T. Nagatsuma (2017), Substorm overshielding electric field at low latitude on the nightside as observed by the HF Doppler sounder and magnetometers, J. Geophys. Res. Space Physics, 122, doi: 10.1002/2017JA024329
- Hashimoto, K. K., T. Kikuchi, I. Tomizawa, K. Hosokawa, J. Chum, D. Buresova, M. Nose and K. Koga (2020), Penetration electric fields observed at middle and low latitudes during the 22 June 2015 geomagnetic storm, Earth, Planets and Space, https://doi.org/10.1186/s40623-020-01196-0
- Kikuchi, T., H. Luehr, K. Schlegel, H. Tachihara, M. Shinohara, and T.–I. Kitamura (2000), Penetration of auroral electric fields to the equator during a substorm, *J. Geophys. Res.*, 105, 23,251-23,261.
- Kikuchi, T., T. Araki, K. K. Hashimoto, Y. Ebihara, T. Tanaka, Y. Nishimura, G. Vichare, A. K. Sinha, J. Chum, K. Hosokawa, I. Tomizawa, Y. Tanaka, A. Kadokura (2022a), Instantaneous achievement of the Hall and Pedersen-Cowling current circuits in northern and southern hemispheres during the geomagnetic sudden commencement on 12 May 2021, Front. Astron. Space Sci. 9:879314. doi: 10.3389/fspas.2022.879314.
- Kikuchi, T.; Hashimoto, K.K.; Tanaka, T.; Nishimura, Y.; Nagatsuma, T. (2022), Middle Latitude Geomagnetic Disturbances Caused by Hall and Pedersen Current Circuits Driven by Prompt Penetration Electric Fields. Atmosphere 2022, 13, 580. https://doi.org/10.3390/atmos13040580

Progress report on the imaging receiver system at the SuperDARN Hokkaido East radar (2025)

Nozomu Nishitani¹, Yoshiyuki Hamaguchi¹, Tomoaki Hori¹, and Shota Hayamizu¹ *Institute for Space-Earth Environmental Research, Nagoya University*

Our group has been working on the implementation of imaging capability to the SuperDARN Hokkaido East radar, operated by Nagoya University.

A typical SuperDARN operating mode is the normal scan program, which scans the entire radar field of view every 1 to 2 minutes. Conventional SuperDARN radars typically have a single receive channel (scanning one beam direction at one time). Therefore, the typical Nyquist frequency for conventional normal scan SuperDARN radar data is 4 to 8 mHz. This time resolution is not suitable for dealing with short term variations such as Pi2 / Pc3 pulsations or space ionospheric disturbances.

Recently, some of the SuperDARN radars have been introducing the imaging receiver systems, which record multiple beam directions simultaneously (e.g., Bristow et al., 2019; McWilliams et al., 2023). Our group at ISEE, Nagoya University, is also preparing this new capability to be implemented at the SuperDARN Hokkaido East radar and is planning to conduct an initial experiment by the end of this year.

The new image receiver system is expected to be able to acquire data with temporal and spatial resolutions several times higher than those of the existing systems. With the new system, we expect to deal with the following topics: (a) Study of a variety of scientific phenomena, such as ULF waves (e.g., Pi2 / Pc3) with periods shorter than 1 minute. (b) Transients excited by external (IMF / solar wind) and internal (e.g., onset of substorm expansion) environmental changes in the ionosphere and magnetosphere. (c) Ionospheric disturbances caused by sudden changes in the earth's surface, such as earthquakes and volcanic eruptions.

In this presentation, we show the latest progress report on this system. This system utilizes the USRP-N210 SDR unit used in the remote receiver for the SuperDARN Hokkaido East radar signal in Nagoya (Nishitani et al., 2021). We have developed a 20-channel, full-specification system, which is currently being tested at the ISEE laboratory and will be sent to the radar site once the system is complete. We are conducting the final calibration of the receiver hardware and are almost ready for the shipping of the whole system to the radar site for initial testing.

References:

Bristow, W. A. (2019). Application of RADAR imaging analysis to SuperDARN observations. Radio Science, 54, 692–703. https://doi.org/10.1029/2019RS006851

McWilliams, K. A., Detwiller, M., Kotyk, K., Krieger, K., Rohel, R., Billett, D.D., et al. (2023). Borealis: An advanced digital hardware and software design for SuperDARN radar systems. Radio Science, 58, e2022RS007591. https://doi.org/10.1029/2022RS007591
Nishitani, N., Y. Hamaguchi, and T. Hori (2021) Development of remote HF wave receiver in the backlobe direction of the SuperDARN Hokkaido East radar: Initial observations. Polar Sci. https://doi.org/10.1016/j.polar.2021.100669

AuroraX project: Current status of 2025

Ryuho Kataoka¹, and AuroraX team²

¹Okinawa Institute of Science and Technology

²AJ1007 project member

We report the current status and some highlighted resuts of so-called AuroraX project. We succeeded to finalize the muon detector observation of Syowa Station in JARE66. Also, we successfully started all-sky camera observations at Casey, Davis, DDU, and Concordia Stations with the help of AAD and IPEV researcher conterparts. During the current solar maximum, we fortunately succeeded to observe several large Forbush events and magnetic storm events. Further, in JARE67, we will start a new Leader-Fraction observation of neutron at Syowa Station to measure the spectral index of galactic cosmic rays. The cutting-edge data assimilation studies utilizing SuperDARN observation are also ongoing in parallel to the new observations. We will discuss what we focus on the last two years of the AuroraX project, combining all of the hard/soft development helitages.

SuperDARN Data Assimilation for Isolated Substorm Dynamics : Machine Learning Emulator Approach

B Nilam¹, Ryuho Kataoka¹, Shinya Nakano², Sachin A Reddy³, Shigeru Fujita², Akira Sessai Yukimatu⁴ Aoi Nakamizo⁵

¹Okinawa Institute of Science and Technology, Okinawa, Japan

²Institute of Statistical Mathematics, Tachikawa, Tokyo, Japan

³Jet Propulsion Laboratory, California Institute of Technology, Pasadena, CA, USA

⁴National Institute of Polar Research, Tachikawa, Tokyo, Japan

⁵National Institute of Information and Communications Technology, Koganei, Japan

The auroral current system is a key component of magnetosphere—ionosphere coupling and plays a significant role in thermospheric dynamics through Joule heating, which enhances satellite drag. Understanding and forecasting this system aids in mitigating space weather impacts on the near-Earth environment. In this study, we present a novel approach to estimate the auroral electrojet indices AL and AU by integrating the machine-learning based emulator named SMRAI, Surrogate Model of REPPU Auroral Ionosphere (Kataoka et al., 2024b, *Space Weather*) with an advanced data assimilation (DA) technique that incorporates observations from the SuperDARN (Nakano et al., 2025, submitted to *Space Weather*). The performance of the SMRAI-DA system is evaluated using a set of isolated substorm events, selected based on the criteria defined by Ohtani and Gjerloev (2020) and constrained by sufficient availability of SuperDARN line-of-sight velocity measurements. The results indicate that assimilating SuperDARN data improves the estimation of the AL and AU indices, as the SMRAI2.1-DA can update both the onset of substorm and its amplitude through the incorporation of SuperDARN data. The current study examines the time evolution of realistic 2D patterns of electric potential associated with the isolated substorms.

Formation of the LLBL in M-I convection unde the northward IMF

IMF 北向きの時の M-I 対流と LLBL の成因

<u>Takashi Tanaka¹</u>
¹Kyushu University, ¹REPPU code Institute

Abstract

Adopting REPPU (REProduce Plasma Universe) code level 8, we reproduced the solar wind-magnetosphereionosphere (S-M-I) interaction when the interplanetary magnetic field (IMF) is obliquely northward, and investigated the relationship between the low-latitude boundary layer (LLBL) and the projection structure of ionospheric convection cells. When the IMF is obliquely northward, the ionospheric convection cells consist of a central lobe + round merging cell (which constitutes the exchange cycle), a reciprocal cell on the opposite side in the morning and evening, a nighttime cell, and two viscous cells at low latitudes. In the magnetosphere, the medium-speed LLBL is formed between the high-speed solar wind and the low-speed magnetospheric interior. From the connection of magnetic field lines, the outer half of the LLBL is projected onto the lobe cell, and the inner half onto the round-merging cell. From the origin of the lobe + round merging cell, it is estimated that both the open and closed magnetic field lines in the LLBL have been the IMF until recently, and especially the open magnetic field lines in the outer half have been the solar wind until more recently. It is not surprising that the LLBL contains particles similar to solar wind particles. Such projection structure is consistent with satellite observations which show that the outer half of the LLBL only appears when the IMF is northward, and that the nature of the particles is more similar to magnetosheath particles. These results indicate that the LLBL is a passway for antisunward convection involving an open magnetic field. The LLBL is Kevin-Helmholtz (KH) unstable, and KH waves propagating along the inner boundary of the LLBL penetrate deep into the magnetosphere. This wave can drive two viscous cells, one in the morning side and one in the evening side, which consist only of closed magnetic field.

REPPU (REProduce Plasma Universe)コードレベル8によって、interplanetary magnetic field (IMF)斜め北向きの時の太陽風一磁気圏一電離圏(S-M-I)相互作用を再現し、low-latitude boundary layer (LLBL)と電離圏対流セルの投影関係を調べた。IMF 斜め北向きの時、電離圏対流セルは中央のローブ+(交換サイクルを構成する)round merging セル、それと朝夕反対側にある reciprocal セル、夜間セル、低緯度の2つの粘性セルの計5つからなる。磁気圏では高速の太陽風と低速の磁気圏内部の間に、中速度の LLBLが形成される。磁力線の接続から、LLBLの外半分はローブセルに、内半分は round-merging セルに投影される。ローブ+round merging セルの成因から推定すると、LLBL にある開磁力線と閉磁力線は、共に最近まで IMF であったものであり、特に外半分の開磁力線はより最近まで太陽風であったものと推定される。LLBL に太陽風粒子に似た粒子が存在するのは当然である。この投影構造は、LLBL の外半分は IMF 北の時のみ現れ、粒子の性質はよりマグネトシース粒子に近いという衛星観測とも、consistentである。これらの結果は、LLBL とは開磁場を含む反太陽向き対流のルートであることを示している。LLBLは Keivin-Helmholtz (KH)不安定であり、LLBL の内側境界に沿って伝搬する KH 波は、磁気圏内部に深く浸透する。これによって、閉磁場のみからなる、朝夕2つの粘性セルが駆動される。

Topological interpretation of the closed and interplanetary magnetic flux interlinkage in the magnetotail during northward interplanetary magnetic field periods

Masakazu Watanabe¹, Takashi Tanaka¹, Dongsheng Cai², and Shigeru Fujita³

¹Kyushu University

²Nagoya University of Commerce and Business

³Research Organization of Information and Systems

The global magnetic field topology the magnetosphere is given by the so-called 2-null, 2-separator structure which is obtained by superposing a dipole field representing the Earth's intrinsic magnetic field and a uniform field representing the interplanetary magnetic field (IMF). In global magnetohydrodynamic simulations for northward IMF, interlinkage of closed and interplanetary magnetic flux is sometimes found in the magnetotail. This indicates that the basic 2-null, 2-separator structure of the magnetosphere is broken. However, the exact magnetic topology responsible for such tangling is still unclear, due to the complexity of the three-dimensional structure, together with the numerical errors in simulation. One key point is the location of the new magnetic nulls that are breaking down the 2-null, 2-separator structure. Nevertheless, the new nulls have never been identified so far in simulations. We here propose a theoretical model in which the new nulls appear near the two original nulls that constitute the 2-null, 2-separator structure. That is, the original magnetic null (one in each hemisphere) multiplexes to form a null cluster (null region), and the magnetic flux interlinkage is formed within the null region. The simplest magnetic topology of the clustering is a 4-null, 8-separator structure, with two nulls in each hemisphere and eight separators connecting them. If we trace the reconnection sequence expected in the 4-null, 8-separator structure from the simulation results, the formation process of the magnetic flux interlinkage is obtained in a natural way. The key process is IMF-lobe reconnection that occurs simultaneously in both hemispheres (the so-called dual lobe reconnection, DLR). In the 2-null, 2-separator structure, IMF-lobe reconnection normally occurs independently in one hemisphere and in the other hemisphere, with the whole space divided by a plane on which the two separators are contained. Thus, the magnetic flux circulations in the two hemispheres are independent. The DLR, however, mixes the magnetic flux circulations in the two hemispheres. Therefore, a steady magnetic flux circulation is no longer maintained. We suggest that this is a trigger of the magnetic null multiplication.

Relationship between the solar wind-magnetosphere structure and IMF parameters in the northward IMF conditions

Shigeru Fujita¹ Takashi Tanaka², Masakazu Watanabe^{3,2}, and Dong Sheng Cai⁴

¹ The Institute of Statistical Mathematics, ROIS

² International Research Center for Space and Planetary Environmental Science, Kyushu University

³ Department of Earth and Planetary Sciences, Faculty of Science, Kyushu University

⁴ Graduate School of Science and Technology, University of Tsukuba

Fujita et al. [2025] discussed the quasi-steady magnetic field structure of the solar wind-magnetosphere system under northward IMF conditions. Their discussion was framed from the perspective of the interaction between magnetic topology and plasma dynamics. In addition, they demonstrated that the vacuum magnetic field, which is produced by the superposition of the Earth's dipole field and the IMF, preserves the fundamental topological form of the solar wind-magnetosphere system. This topology provides the fundamental magnetic field structure necessary for magnetic reconnection between the IMF and the Earth's magnetic field. They further pointed out that the vacuum magnetic field represents the ground state of the system. Based on this finding, they argued that the quasi-steady magnetic field structure is determined by the balance between two forces: the deformation force exerted by plasma and the restoring force that tends to return the field to its ground state. Furthermore, the magnetic reconnection process is inherently built into this magnetic structure. From this viewpoint, the process of magnetic reconnection is naturally incorporated into the overall description.

Based on the theoretical framework described above, we now examine variations in the solar wind-magnetosphere system that depend on the IMF parameters under northward IMF conditions. Our discussion focuses on the following four aspects.

- 1. An increase in the IMF intensity results in a shorter plasma sheet. At the same time, the convection speed within the plasma sheet becomes faster.
- 2. Under intensified IMF conditions, a high-speed plasma flow develops in the magnetosheath.
- 3. The theta aurora, associated with a reversal of the IMF By component, becomes more distinct when the IMF intensity is strong.
- 4. When the IMF is very weak, magnetic null points can appear outside the bow shock. In this case, the magnetosphere-ionosphere convection exhibits a two-cell pattern, which is typically seen under southward IMF conditions.

Impact of downward propagating planetary waves associated with sudden stratospheric warming on the extratropical troposphere: zonal wavenumber 1 component

Yuki Kojima¹, Hitoshi Mukougawa¹ Graduate School of Science, Kyoto University, Kyoto, Japan

To elucidate characteristics of significant downward propagation (SDP) of WN1 planetary waves from the stratosphere after SSW events and their influence on the extratropical circulation in the troposphere, we conducted a case study of a distinct SDP event in March 2023 as well as composite analyses for SDP events with and without SSW over 66 winters, using JRA-3Q reanalysis dataset provided by the Japan Meteorological Agency. The SDP event was defined as occurring when the vertical component of the 100-hPa WN1 E-P flux averaged north of 60°N was negative and less than one standard deviation below the climatological mean for at least five consecutive days. Additionally, SDP events occurring within 20 days after the central date of an SSW event were classified as SDP events with SSW. The remaining SDP events were classified as SDP events without SSW. A total of 18 SDP events with SSW and 55 SDP events without SSW were identified.

A case study of the SDP event in March 2023, which was classified as an SDP event with SSW, revealed the equatorward propagation of enhanced WN1 components in the troposphere from the polar regions after the downward propagation with an eastward phase tilt up to the mid-stratosphere. It was also found that the WN1 downward propagation began when the stratospheric zonal winds were easterly in association with the preceding SSW. During the equatorward propagation period, East Asia, including Japan, was covered by the WN1 ridge with a southwest–northeast phase tilt, contributing to the unusually high temperature anomalies observed over Japan.

Then, we statistically explored the potential impact of the SSW on SDP events using a bootstrap method. We found that an SDP event is significantly more likely to occur after an SSW than would be expected by chance. On the other hand, the SSW does not affect the mean duration of SDP events.

Next, the uniqueness of the SDP event with SSW in March 2023 was examined by comparing it with the composites for all SDP events with SSW and those without SSW. The composite was constructed based on the onset date (Day 0) of each SDP event, that was defined as the first day on which the vertical component of the 100-hPa E-P flux met the SDP event criterion. Moreover, before compositing the WN1 component, the associated wave fields were shifted so that the 500-hPa WN1 ridge at high latitudes on Day 0 was aligned with the prescribed longitude. This procedure made the composited wave structure clear despite the significant variation in the WN1 phase depending on the SDP event.

The temporal evolution of the composited WN1 components for SDP events with SSW is summarized as follows. The downward propagation of stratospheric WN1 components initiates when the stratosphere zonal winds are easterly associated with the preceding SSW. The WN1 phase tilts eastward up to upper stratosphere. Then, tropospheric WN1 components, amplified in the polar region during the onset period of the downward propagation, propagate equatorward and produce temperature anomalies in the extratropical troposphere depending on the WN1 phase on Day 0 in high latitudes: When the WN1 ridge is located around the date line, cold anomalies cover East Asia, including Japan; As the WN1 ridge shifts away from the date line longitudinally, warm anomalies tend to cover East Asia. The preference of the WN1 ridge over the North Pacific sector was also seen, which is consistent with the blocking preference for reflecting SSWs in that sector as revealed by Kodera et al. (2016). The SDP event with SSW in March 2023 shows similar time evolution to the composite SDP event with SSW. However, among the SDP events with SSW, the WN1 components in high latitudes exhibit the greatest amplitude and the largest phase shift from the date line. The extraordinary characteristics of downward propagated WN1 components would contribute to the extremely warm anomalies over Japan in March 2023.

The SDP events without SSW are highlighted by the prevalence of stratospheric westerly winds during the downward propagation of the WN1 component. Despite the discrepancy in the basic wind profile, the WN1 components during the SDP events without SSW exhibit similar time evolution to those during the SDP events with SSW except for the following differences in the WN1 characteristics: much larger amplitude in the upper stratosphere, vertically restricted eastward phase tilt up to the middle stratosphere, and weaker meridional phase tilt associated with the equatorward propagation in the troposphere. Consequently, cold anomalies tend to occur in East Asia when the WN1 ridge in polar regions is located at 120°E on Day 0.

The significant difference in the configuration of stratospheric zonal-mean zonal winds between the SDP events with and without SSW suggests another mechanism besides the wave reflection mechanism proposed by Shaw and Perlwitz (2013) that explains the occurrence of downward propagation of stratospheric WN1 components. We also discuss the synoptic conditions of tropospheric circulation during the winter of 2023 in relation to the extraordinary amplification of WN1 components.

References

Kodera K, Mukougawa H, Maury P, Ueda M, Claud C, Absorbing and reflecting sudden stratospheric warming events and their relationship with tropospheric circulation. J. Geophys. Res.: Atmos., 121, 80–94, 2016. Shaw TA, Perlwitz J, The life cycle of northern hemisphere downward wave coupling between the stratosphere and troposphere. J. Climate, 26, 1745–1763, 2013.

Short-period height variation of a sporadic Ca⁺ layer

Azusa Yamakawa¹, Mitsumu K. Ejiri¹², Takuji Nakamura¹², Takuo T. Tsuda³, Takanori Nishiyama¹², Makoto Abo⁴, Katsuhiko Tsuno⁵, Takayo Ogawa⁵, and Satoshi Wada⁵

¹SOKENDAI (The Graduate University for Advanced Studies), Japan

²National Institute of Polar Research (NIPR), Japan

³University of Electro-Communications (UEC), Japan

⁴Tokyo Metropolitan University, Japan

⁵RIKEN (The Institute of Physical and Chemical Research), Japan

Sporadic E layers (EsL) occurring in the ionospheric E region at altitudes of 90–150 km are thin layers only a few kilometers thick. They have very high electron density and also contain abundant metallic ions. EsL cause radio communication disturbances in the HF/VHF bands. Therefore, elucidation of the mechanisms of EsL formation and evolution is important. In the mid-latitudes, EsL have been understood to be formed by convergence of metallic ions in the ionospheric E region driven by the vertical shear of neutral horizontal winds and the geomagnetic field. Because observation of the spatiotemporal structure of EsL is limited, their morphological variations and lifecycle are not yet well understood. The primary source of metals in the ionospheric E region is meteors, and there are layers of metallic atoms and ions such as iron, magnesium, sodium, calcium, and so on. Among these species, calcium ion (Ca⁺) is the only metallic ion that can be detected from the ground by resonance scattering lidar.

The National Institute of Polar Research (NIPR) developed a frequency-tunable resonance scattering lidar and carried out Ca⁺ observations at Tachikawa in Japan (2014–2016) and at Syowa Station in the Antarctic (2017–2018). In this study, we analyzed a sporadic Ca⁺ layer on September 1, 2016 at Tachikawa (35.7°N, 139.4°E), focusing on a periodic height variation of the Ca⁺ layer identified at altitudes of 99–101 km between 15:55 and 16:20 UT. The Ca⁺ density profiles had height and time resolutions of 165 m (smoothed from 15 m resolution data) and 5 s, respectively. We derived the centroid altitude of each Ca⁺ density profile and fitted its temporal variation with a sinusoidal curve. From this fitting, the vertical displacement amplitude and the observed (ground-based) oscillation period were estimated to be 170 m and 7.5 minutes, respectively. We then applied the dispersion relation of internal gravity wave together with the relation between observed and intrinsic frequencies to derive gravity wave parameters, including horizontal wavelength and phase velocity, that are consistent with the observed oscillation. Vertical wavelength and the background wind speed were assumed, the latter of which was considered referring to the JAWARA reanalysis data of corresponding time and altitude. Our investigation suggested that the wave propagation direction was in the same direction as the background wind rather than the opposite direction, when the observed oscillation is caused by internal gravity waves.

Long-term variation of the back-ground wind field in the Antarctic MLT region

Masaki Tsutsumi^{1,2}
¹National Institute of Polar Research
²SOKENDAI

The middle frequency (MF) radar at Syowa station, Antarctica (69S, 39E), has continuously been observing horizontal winds in the mesosphere and lower thermosphere since 1999. In addition to the conventional correlation analysis wind measuring technique [Briggs, 1984], a meteor wind technique has also been adopted for the Syowa system [Tsutsumi and Aso, 2005]. Because of its low radio frequency (2.4 MHz) the MF meteor winds can be estimated up to 120 km in contrast to the conventional VHF (~30 MHz) meteor radars, where the upper limit is around 105 km. In this study we examine the long-term variation of the Antarctic mesosphere and lower thermosphere winds based on the quarter century of data, with an emphasis on the lower thermosphere, where a long-term wind trend has rarely been estimated because of the lack of such long period of wind data.

References

Briggs, B. H. (1984), The analysis of spaced sensor records by correlation techniques, in Handbook for MAP, vol. 13, pp. 166 – 186, SCOSTEP

Tsutsumi and Aso, MF radar observations of meteors and meteor-derived winds at Syowa (69S, 39E), Antarctica: A comparison with simultaneous spaced antenna winds, JOURNAL OF GEOPHYSICAL RESEARCH, VOL. 110, D24111, doi:10.1029/2005JD005849, 2005

Modulation of the mid-latitude ionospheric Sporadic E layer by the polar vortex

Tomoki Maeda¹, Huixin Liu¹, Yosuke Yamazaki², Lihui Qiu¹

¹ Kyushu University

2. Leibniz Institute of Atmospheric Physics at the University of Rostock

The sporadic E (Es) layer, a thin ionospheric layer of metallic ions, is a prominent phenomenon in the atmosphere—ionosphere coupling system, mainly driven by vertical shear of neutral winds at mid-latitudes. In this study, we statistically investigate for the first time the relationship between Es and the strength of the northern polar vortex during December-February (represented by the Northern Annular Mode,NAM, index), using 19 years of ionosonde observations over Japan and Australia. Our analysis reveals a negative dependence of Es intensity on the NAM index, especially clear in the afternoon sector. In contrast, no clear relationship between NAM and Es intensity is seen in Australia, implying the impacts of the northern polar vortex is limited to the northern hemisphere. These findings suggest polar vortex modulation of ionospheric Es irregularities via semidiurnal tides. Thus, the polar vortex, especially NAM index, may be a useful parameter for forecasting Es variability.

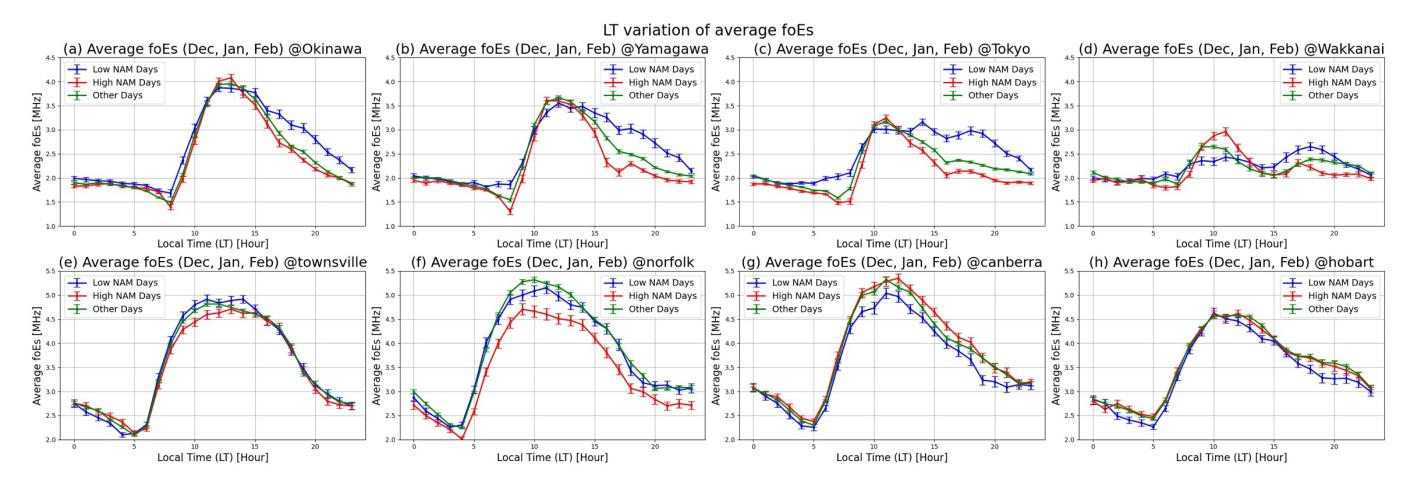


Figure 1. Local time variation of the average foEs under difference NAM conditions.

References

Andoh, S., Saito, A., & Shinagawa, H. (2024a). Physical mechanism for the temporary intensification of wintertime sporadic E layers in 2009. Earth, Planets and Space, 76, doi: 10.1186/s40623-024-01966-0

Andoh, S., Saito, A., & Shinagawa, H. (2024b). Sporadic E layer intensification in the winter of 2009 examined by FORMOSAT-3/COSMIC RO data and GAIA model. Journal of Geophysical Research: Space Physics, 129, e2024JA033026. doi: 10.1029/2024JA033026

Haldoupis, C. (2011), Midlatitude Sporadic E. A Typical Paradigm of Atmosphere-Ionosphere Coupling. Space Sci Rev, 168:1–21. doi: 10.1007/s11214-011-9786-8

Characteristics of Quasi-Co-rotating Auroras Observed on the Ground

Yukino Sato^{1,2}, Yoshimasa Tanaka^{1,2,3}, Ryuho Kataoka^{2,4}, Takanori Nishiyama^{1,2}, Yasunobu Ogawa^{1,2,3}
¹SOKENDAI, ²NIPR, ³ROIS-DS, ⁴OIST

Auroras with unusual stationary patches were first reported at Poker Flat Research Range (PFRR), Alaska, in October 2000 and were named the "Evening Corotating Patch (ECP) aurora" [Kubota et al., 2003]. The ECP aurora appeared on the equatorward side of the auroral oval (L = 5-8) and was mainly observed at OI 557.7 nm and N2+ 427.8 nm, consistent with the precipitation of several to ~10 keV electrons. Subsequently, Toyoshima (2003) identified 44 similar events and named them "Quasi-Corotating (QC) aurora." Due to geographical restrictions, previous studies have been scarce, and the statistical characteristics are poorly understood.

We present a statistical analysis of QC auroras using data from a monochromatic 391.4 nm all-sky camera at Syowa Station, Antarctica (2023–2024). We identified 23 events that occurred in the evening sector (until 20 MLT) and retained their shape and position for more than 20 minutes. Their occurrence peaked around 15 MLT, earlier than previously reported, and most events occurred under quiet conditions (Kp = 1–3), consistent with Toyoshima (2003). Furthermore, in September 2025, we plan to install an all-sky camera equipped with multi-wavelength band-pass filters at PFRR, Alaska, to initiate new observations of the QC aurora. In this presentation, we also report the analysis results from Syowa Station, together with an overview of the auroral observation system to be deployed.

References

- [1] Kubota, M., et al. (2003), Evening co-rotating patches: A new type of aurora observed by high sensitivity all-sky cameras in Alaska, Geophys. Res. Lett., 30(12), 1612. https://doi.org/10.1029/2002GL016652
- [2] Toyoshima, S. (2003), Characteristics of Quasi-corotating Aurora and Remote Sensing of Magnetospheric Dynamics. Master Thesis, Department of Geophysics, Tohoku University, Japan

Reconstruction of the three-dimensional structure of the Westward Traveling Surge

<u>Tau Hoshino</u>¹, Yoshimasa Tanaka^{1,2,3}, Yasunobu Ogawa^{1,2,3}, Takanori Nishiyama^{1,2}, Keisuke Hosokawa⁴, Kirsti Kauristie⁵, Alexander Kozlovsky⁶, Tero Raita⁶

SOKENDAI¹, NIPR², ROIS-DS³, The University of Electro-Communications⁴, Finnish Meteorological Institute⁵, Sodankyla Geophysical Observatory, University of Oulu⁶

Auroras occur when charged particles precipitating from the Earth's magnetosphere collide with the upper atmosphere, exciting atmospheric constituents and producing light emissions. The aurora follows a characteristic development process known as an auroral substorm. During a substorm, the aurora expands explosively both poleward and in the east–west direction. Among these, the expansion particularly toward the west is called the Westward Traveling Surge (WTS). WTS is the most prominent phenomenon of a substorm, and its development has been discussed within various models. However, the expansion and propagation speed of WTS is as fast as ~1 km/s, and no observational studies to date have investigated the spatiotemporal evolution of its three-dimensional structure. In this study, we aim to quantitatively examine the three-dimensional structure of WTS, as well as the horizontal distribution of precipitating electron energy, using the generalized aurora tomography method [1]. Aurora tomography applies the principles of computed tomography to reconstruct the three-dimensional auroral structure from multiple simultaneous images captured at different observation sites.

Specifically, we determined the differential flux of precipitating electrons by minimizing the residuals between image data and model calculations, from which the three-dimensional emission intensity distribution was derived. In this process, hyperparameters such as the relative sensitivity of the image data and the weighting of the regularization term need to be set in advance, and we determined them using cross-validation. By reconstructing the three-dimensional structure, it becomes possible to quantitatively discuss physical parameters of WTS, such as the electron density distribution and conductivity distribution in WTS from an observational perspective. The validity of the reconstructed electron density distribution can be verified by direct comparison with measurements obtained from the EISCAT radar. As a future objective, we aim to extend the discussion to include the three-dimensional current system of WTS and its consistency with theoretical models.

In this presentation, we report the results of tomography analysis applied to auroral image data at 427.8 nm wavelength obtained from Tromsø (69.58°N, 19.23°E), Abisko (68.36°N, 18.82°E), and Kilpisjärvi (69.05°N, 20.36°E) for a WTS event observed around 22:45:34 UT on February 16, 2018. We present the hyper parameter, energy scale of differential flux and its distribution of precipitating electrons and three-dimensional structure of this WTS event.

References

[1] Y. Tanaka et al., Ann. Geophys., 29, 551 (2011).

Assessing interference of various vehicles in the geomagnetic absolute measurement - toward optimizing their access restrictions at Syowa Station.

Tomoyuki Yara¹, Junpei Oogi¹, Shin Arita¹, Tomomi Inamura², Hideyuki Hirahara¹ and Akira Kadokura^{3,4}

¹Kakioka Magnetic Observatory, Japan Meteorological Agency, Japan

²Atmosphere and Ocean Department, Japan Meteorological Agency, Japan

³Polar Environment Data Science Center, ROIS-DS, Japan

⁴National Institute of Polar Research, Japan

Vehicles such as snowcat, snow groomer and heavy machinery contain a substantial amount of iron, and hence have an intrinsic magnetic moment. Artificial magnetic fields generated by those vehicles can affect geomagnetic observations seriously. At Syowa Station, Antarctica, vehicle access is therefore restricted around the Geomagnetic Observation Hut to avoid the magnetic interference during the weekly "geomagnetic absolute measurement". The restriction area has been uniformly defined by empirical rules, without any quantitative assessment of the specific amount of impact that each vehicle would have on the Geomagnetic Observation Hut. Since the magnetic moments vary with each individual vehicle, some may be restricted excessively. While the restrictions are necessary for conducting the observations, they impose limitations on the operation of the expedition.

The goal of this study is to contribute to a smoother operation of the expedition by considering appropriate access restrictions for each vehicles. To that end, we evaluate the magnetic moments of vehicles at Syowa Station so that the restriction can be optimized by individually taking into account their impacts on the Geomagnetic Observation Hut.

In determining the magnetic moment we had to fulfill necessary measurements with a minimum amount of effort required (e.g., number of measurement points, measurement time, travel distance) because of the multiple constraints on the station, such as personnel, instruments, time, and climate. Therefore we developed an efficient method to estimate the magnetic moment of a vehicle from a change of the total magnetic force before and after its parking. It was found that a magnetic moment with sufficient accuracy for practical use can be obtained even with the measurements at three points (i.e. the minimum number of data theoretically required for the analysis), unless two or more measurement points are arranged in a straight line with the vehicle.

During the wintering period of JARE65, we attempted to evaluate the magnetic moment of 17 vehicles, consisting mainly of large vehicles such as SM100S and PB300S at Syowa Station. The total magnetic force measurements were carried out using a proton magnetometer at five points in the test field. We will report on the results.

Magnetospheric-density estimation using FLRs in both ionospheric and ground/sea backscatters of SuperDARN VLOS in a consistent manner with the aid of the DTFT

Hideaki Kawano¹, Akira Sessai Yukimatu², Nozomu Nishitani³, Yoshimasa Tanaka², and Tomoaki Hori³

¹International Research Center for Space and Planetary Environmental Science, Kyushu University, Japan

²National Institute of Polar Research, and Polar Science Program, SOKENDAI, Japan

³Institute for Space-Earth Environmental Research, Nagoya University, Japan

Where the frequency of waves coming into the magnetosphere matches the eigenfrequency of a geomagnetic field line, which runs through the ground, the ionosphere, and the magnetosphere, FLR (field-line resonance) can cause the eigen-oscillations of the field line. By using the frequency of the eigen-oscillation, called the FLR frequency, one can estimate the density along the magnetic field line, because, in a simplified expression, 'heavier' field line oscillates more slowly.

Since the pulsations oscillate the ionospheric plasma, too, there could exist cases in which SuperDARN radars monitor the two-dimensional (2D) distribution of the FLR frequency, from which we can estimate 2D plasma-density distribution on the magnetospheric equatorial plane, including the location of the plasmapause. However, visual identification of the FLR in the SuperDARN VLOS (Velocity along the Line of Sight) data is time-consuming, and the visual identification could miss small-amplitude FLR events and "hidden" FLR events which are superposed by non-FLR perturbations. In addition, there are lots of VLOS data to be analyzed.

Thus, we have been developing a computer code to automatically identify the FLR for any beam of any radars, by using the amplitude-ratio method and the cross-phase methods; these methods cancel out the superposed non-FLR perturbations by dividing the data from a Range Gate (RG) by the data from a nearby RG along the same beam, because the FLR frequency tends to depend on the latitude more strongly than the superposed non-FLR perturbations. Another advantage of applying these methods to the SuperDARN VLOS data is that we can choose any pair of RGs (along the same beam) with different distances, and thus can identify what distance is the best to identify the FLR. This distance reflects the resonance width, which is an important quantity reflecting the diffusion and dissipation of the FLR energy. In the early phase of the code development, we confirmed that the code identified FLR events which we had visually identified in a few beams of a few radars.

The code needs to automatically distinguish whether the identified FLR was in the ionospheric backscattered signal or in the ground/sea backscattered signal; for the latter, the code needs to find the ionospheric reflection point, which is the actual location of the observed FLR. We implemented these features and tested them for a few radars, and found that the ground/sea events tended to be located at latitudes fairly lower than those of simultaneously-observed ionospheric events. We also calculated, for each event, the corresponding magnetospheric equatorial density, and found that the ground/sea events tended to show pretty much lower density than the ionospheric events located at similar latitudes. We thought that these differences could come from the pretty low frequency resolution of the FFT, thus we increased them by using the Discrete-Time Fourier Transform (DTFT) method. As a result, these differences did get smaller. We will implement the DTFT method into our code.

From another viewpoint, there exist more recent, more advanced methods to increase the frequency resolution. We intend to test them and show the results at the presentation.

By using the code we expect to identify much more FLR events than by visual identification; the automatically identified FLR events would include events simultaneously observed at several locations by several radars, increasing the possibility of monitoring the 2D distribution of the plasma density on the magnetospheric equator and identifying magnetospheric regions.

Preliminary evaluation of electron acceleration by whistler-mode waves in Mercury's magnetosphere using test particle simulations

Takahiro Watanabe¹, Mitsunori Ozaki¹ and Satoshi Yagitani¹

**IKanazawa University, Kanazawa, Japan

Mercury, like Earth, possesses an intrinsic magnetic field, and its magnetosphere is thought to exhibit a spatial structure like that of Earth's magnetosphere. Whistler-mode waves have been observed within Mercury's magnetosphere, and wave–particle interactions are expected to produce electron acceleration and corresponding energy variations, as is known to occur in Earth's magnetosphere. On the other hand, since Mercury and Earth differ greatly in planetary magnetic field strength and solar wind conditions, comparing their magnetospheric scales may help distinguish Mercury-specific phenomena from universal mechanisms.

In this study, to investigate the universality of electron acceleration caused by wave–particle interactions with whistler-mode waves in Mercury's and Earth's magnetospheres, we first examined the scaling law of magnetospheric size. Unlike conventional scaling based on the magnetopause standing distance, our analysis focused on the magnetic field inhomogeneity, which plays a critical role in the nonlinear growth of whistler waves. As a result, the value of the magnetospheric scaling factor was found to be approximately 7.6±0.4, suggesting that Mercury's magnetosphere corresponds to a region equivalent to that outside Earth's radiation belts. Furthermore, we investigated electron acceleration through wave–particle interactions with whistler-mode waves in both Earth's and Mercury's magnetospheres using test particle simulations. The simulation results revealed that the energy gain in Earth's magnetosphere is about 10 to 100 times greater than in Mercury's, and while energy gain at Earth occurs over a pitch-angle range of approximately 70°, it is confined to a much narrower range of about 10° at Mercury.

In this presentation, we will discuss the differences in electron acceleration characteristics driven by whistler-mode waves between Mercury and Earth. Future work will incorporate solar wind conditions and comparative analysis using observational data.

Test Particle Simulations of Electron Precipitation Rates Induced by Whistler-Mode Waves in Mercury's Polar regions

Yuki Detambo¹, Mitsunori Ozaki¹, and Satoshi Yagitani¹

**IKanazawa University, Kanazawa, Japan

Whistler-mode waves are important natural electromagnetic emissions that cause electron acceleration and loss through wave-particle interactions in planetary magnetospheres. These waves are thought to play an important role in the formation and variation of radiation belts, particularly in the Earth's magnetosphere, and their influence is also attracting attention in small magnetospheres such as Mercury's.

In this study, we performed numerical simulations to analyse the interaction between whistler-mode waves and electrons in Mercury's magnetosphere, based on both cyclotron and Landau resonance mechanisms. We then quantitatively evaluated the electron precipitation rate to Mercury's polar regions.

A comparison between cyclotron and Landau resonance at L=1.2 revealed that cyclotron resonance yields an electron precipitation rate 6.6% higher than that of Landau resonance (for 30-deg. oblique propagation). It was also confirmed that in the case of Landau resonance, lower-energy electrons (around 1 keV) contribute more significantly to precipitation than in cyclotron resonance.

For cyclotron resonance at L=1.2, we investigated the effect of wave propagation angle and found that parallel propagation tends to produce an electron precipitation rate 0.48% higher than 30-deg. oblique propagation. Regarding the L-shell dependence of the resonance region, a comparison between L = 1.2 and L = 1.4 showed that smaller L values result in precipitation rates about 2.0% higher. Furthermore, when varying the magnetic latitude λ from -4° to -20° at L=1.2, higher latitudes (larger $|\lambda|$) corresponded to higher precipitation rates. These trends are attributed to the fact that parallel-propagating waves more directly influence electron trajectories, smaller L regions have stronger magnetic fields that promote more efficient resonance, and stronger magnetic convergence at higher latitudes facilitates electron precipitation.

Similarly, for Landau resonance from L=1.1 to 1.5, simulations with varying L values showed that the precipitation rate at L=1.1 produce a 2.4% higher in comparison with that of L=1.5. A comparison of $\lambda=-20^\circ$, 0° , and $+20^\circ$ at L=1.2 revealed that the case of $\lambda=-20^\circ$ exhibits a 0.21% lower precipitation rate than the others. These results suggest that as L decreases, the increased magnetic field strength enhances wave-particle interactions, while the lower precipitation rate at $\lambda=-20^\circ$ may be due to a change in resonance conditions caused by the local increase in magnetic field strength, reducing the number of resonant particles.

In this work, the electron precipitation rates for oblique propagation were evaluated by combining the results from cyclotron and Landau resonance. Future work will include analyses of electron acceleration for both oblique and parallel propagation, thereby contributing to a quantitative understanding of wave-particle interactions in Mercury's magnetosphere.